INSTITUTE OF PHYSICS PUBLISHING JOURNAL OF GEOPHYSICS AND ENGINEERING
J. Geophys. Eng. **3** (2006) 122–134 doi:10.1088/1742-2132/3/2/003

Sharp boundary inversion in crosswell travel-time tomography

M S Zhdanov[1], G Vignoli[2] and T Ueda[1]

[1] University of Utah, Department of Geology and Geophysics, Salt Lake City, UT 84112, USA
[2] Università di Ferrara, Dipartimento di Scienze della Terra, 44100 Ferrara, Italy

E-mail: mzhdanov@mines.utah.edu

Received 21 July 2005
Accepted for publication 16 February 2006
Published 21 March 2006
Online at stacks.iop.org/JGE/3/122

Abstract
The reconstruction of seismic images of the medium from crosswell travel-time data is a typical example of the ill-posed inverse problem. In order to obtain a stable solution and to replace an ill-posed problem by a well-posed one, a stabilizing functional (stabilizer) has to be introduced. The role of this functional is to select the desired stable solution from a class of solutions with specific physical and/or geometrical properties. One of these properties is the existence of sharp boundaries separating rocks with different petrophysical parameters, e.g., oil- and water-saturated reservoirs. In this paper, we develop a new tomographic method based on application of a minimum support stabilizer to the crosswell travel-time inverse problem. This stabilizer makes it possible to produce clear and focused images of geological targets with sharp boundaries. We demonstrate that the minimum support stabilizer allows a correct recovery of not only the shape but also the velocity value of the target. We also point out that this stabilizer provides good results even with a low ray density, when the traditional minimum norm stabilizer fails.

Keywords: inversion, focusing, crosswell, travel-time tomography

1. Introduction

Crosswell tomography is one of the most widely used techniques in geoscience and geoengineering. The crosswell methods are used in petroleum reservoir characterization (Lee *et al* 1995, Williams *et al* 1997), geotechnical applications (Wright *et al* 1988, Yamamoto *et al* 1994, Rechtien *et al* 1995, Hyndman and Harris *et al* 1996) and mining explorations (Pratt *et al* 1993, Wong 2000) where adjacent boreholes are available. In these situations, it is often desirable to have a high-resolution description of the rock formations between the boreholes. In a crosswell seismic survey, a seismic source is placed in one borehole and receivers are located in another borehole. The source is fired and the resulting energy propagates through the rock and is received in the other borehole. The source and receivers are then moved to another position and the firing and receiving process is repeated. This surveying procedure is continued until the region of interest has been adequately traversed by the propagating energy.

There are several advantages of crosswell geometry over surface reflection imaging. Because the propagation of the seismic signal in the near surface layers is often highly attenuated, the high frequencies are degraded upon passage through them. The high-frequency loss in the surface structures reduces the resolution that can be achieved in the final image. For example, the travel-time picking error is inversely dependent on the frequency of the seismic wave. Therefore, the lowered frequencies cause greater picking errors, which results in the creation of the velocity errors.

The reconstruction of the seismic image of the medium from crosswell tomographic data is a typical example of an ill-posed inverse problem. Modern inversion methods are usually based on the Tikhonov regularization theory and provide a stable solution of inverse problems. This goal is reached by introducing the appropriate stabilizing functionals in the inverse problem solution. The main application of the stabilizing functionals (the stabilizers) is in bringing *a priori* information about the desirable properties of the solution into the inversion algorithm.

Over the last decade several different stabilizers have been introduced (Geman and Reynolds 1992, Geman and Yang 1995, Vogel 1997, Lobel *et al* 1997, Portniaguine and Zhdanov 1999, Zhdanov 2002, pp 45–52). These new stabilizers make it possible to produce clearer and more focused images of the inverse model than the traditional maximum smoothness stabilizers. For example, the minimum support (MS) functional was found useful in the solution of geophysical inverse problems (Portniaguine and Zhdanov 1999, Zhdanov 2002, pp 45–52). This functional helps to select the desired stable solution from the class of solutions with specific physical and/or geometrical properties. In geophysical applications, one of these properties is the existence of sharp boundaries separating geological formations with different physical parameters, e.g., oil- and water-saturated reservoirs. The practical problem of sharp boundary inversion with the MS stabilizer is that this functional is non-quadratic, which complicates the minimization of the Tikhonov parametric functional. In the original implementation of the regularized focusing inversion, this problem was overcome by a linear transformation of the model parameters into the space of the weighted model parameters. As a result of this transformation, the MS stabilizer becomes quadratic. This linear transformation is updated from iteration to iteration, which is equivalent to the re-weighting of the model parameters. For example, one can solve the inverse problem using the re-weighted regularized conjugate gradient (RRCG) method with repeated modification of the model parameter weights after every few iterations. The advantage of this approach is in its simplicity. The disadvantage is that, due to re-weighting, the misfit and stabilizing functionals can change and even increase from iteration to iteration (Zhdanov 2002, p 159).

There are different ways to overcome this difficulty. One approach was introduced in the paper by Zhdanov and Tolstaya (2004), where the non-quadratic minimum support stabilizing functional was transformed into a quadratic one by using a specially selected nonlinear transformation of the model parameters based on minimum support nonlinear parametrizations. This technique was successfully tested on the synthetic three-dimensional (3D) magnetotelluric data inversion for an earth conductivity structure.

In the current paper, we consider another approach which solves the same problem using the direct minimization of the Tikhonov parametric functional with the minimum support stabilizer. The advantage of this technique is that it excludes the additional steps of nonlinear transformation from the auxiliary model parameters to the true parameters, which simplifies and speeds up the inversion algorithm. We apply this new technique to the crosswell seismic tomography problem. We compare the results of travel-time inversion obtained using two different types of stabilizing functionals: minimum norm and minimum support stabilizers. We also investigate the sensitivity to noise and the effect of model parameter weights on inversion efficiency.

We should note, however, that the developed algorithm can be applied for a wide range of imaging problems, including electromagnetic imaging and medical imaging.

2. The travel-time inverse problem

For completeness, we begin our paper with a brief overview of the basic principles of travel-time tomography. In the framework of the 'geometric optics' approach to seismic problems, the travel time $\tau(\mathbf{r}', \mathbf{r}_j)$ of the seismic ray can be related to the local seismic velocity $c(\mathbf{r})$ by the relationship

$$\tau(\mathbf{r}', \mathbf{r}_j) = \int_{L(\mathbf{r}', \mathbf{r}_j)} s(\mathbf{r})\, \mathrm{d}l, \tag{1}$$

where $\mathbf{r}$ is the radius-vector of the observation point in some Cartesian system of coordinates, $L(\mathbf{r}', \mathbf{r}_j)$ denotes the raypath between the source $\mathbf{r}'$ and the receiver $\mathbf{r}_j$, and the slowness $s(\mathbf{r})$ is equal to $1/c(\mathbf{r})$.

This equation is, in general, not linear because the raypath $L(\mathbf{r}', \mathbf{r}_j)$ depends on the slowness $s(\mathbf{r})$. However, we can calculate the variation of the travel time using Fermat's principle, which states that the travel time is stationary with respect to a variation of the raypath $L(\mathbf{r}', \mathbf{r}_j)$:

$$\delta\tau(\mathbf{r}', \mathbf{r}_j) = \int_{L(\mathbf{r}', \mathbf{r}_j)} \delta s(\mathbf{r})\, \mathrm{d}l. \tag{2}$$

Let us suppose that we know some background model $s_b(\mathbf{r})$ of the slowness distribution and that the current model $s(\mathbf{r})$ is obtained by a small perturbation of $s_b(\mathbf{r})$:

$$s(\mathbf{r}) = s_b(\mathbf{r}) + \Delta s(\mathbf{r}). \tag{3}$$

In this case

$$\tau(s_b + \Delta s) = \int_{L(s_b+\Delta s)} (s_b + \Delta s)\, \mathrm{d}l \simeq \int_{L(s_b)} (s_b + \Delta s)\, \mathrm{d}l, \tag{4}$$

where $\tau(s_b + \Delta s)$ is the travel-time stationary along the actual raypath, and $L(s_b)$ is the raypath in a homogeneous background medium which is a straight line between the source and the receiver. In this way, the problem becomes linear.

It is possible to discretize the ground with a regular grid with a constant velocity in the L cells. Thus we can introduce a vector $\mathbf{m}$ of the model parameters as a vector of slowness within each cell of the grid:

$$\mathbf{m} = (s_1 s_2 \ldots s_L), \tag{5}$$

and a vector $\mathbf{d}$ of the data as a vector formed by the travel times:

$$\mathbf{d} = (\tau_1 \tau_2 \ldots \tau_N), \tag{6}$$

where τ_i is the first arrival travel time of the ith ray.

As a result, we obtain a linear system of equations for slowness distribution over the grid:

$$\mathbf{d} = \widehat{\mathbf{A}}\mathbf{m}, \tag{7}$$

where $\widehat{\mathbf{A}} = [A_{ij}]$, and component A_{ij} is the distance that the ith ray travels within the jth cell.

3. Tikhonov regularization and stabilizing functionals

The system of linear equations (7) represents a special case of a general linear inverse problem

$$d = A(m), \tag{8}$$

where A is the linear forward modelling operator, $m = m(\mathbf{r})$ is a function of a point $\mathbf{r} \in V$ describing the model parameter distribution in some volume V in the earth ($m \in M$, where

M is a Hilbert space of models with L_2 norm), and d denotes a geophysical data set ($d \in D$, where D is a Hilbert space of data).

The conventional way to find a unique and stable solution of the problem (8) is usually based on the minimization of the Tikhonov parametric functional (Tikhonov and Arsenin 1977):

$$P^{\alpha}(m) = \phi(m) + \alpha s(m), \tag{9}$$

where ϕ is the misfit functional defined as the norm of the difference between the observed and predicted data:

$$\phi(m) = \|A(m) - d\|^2_{L_2}, \tag{10}$$

and functional $s(m)$ is the stabilizing functional, whose function is to select a correctness subset M_c from the space of all possible models M. In this way an ill-posed problem becomes well posed.

There are several different possible choices for the stabilizer (Zhdanov 2002). In this paper, we analyse just two of them.

(1) The minimum norm stabilizer (s_{MN}), which is equal to the difference between the current model m and an appropriate *a priori* model m_{apr}:

$$s_{\mathrm{MN}}(m) = \|m - m_{\mathrm{apr}}\|^2_{L_2};$$

(2) The minimum support stabilizer (s_{MS}), which is proportional to the area (support) of the nonzero values of the difference between the current model m and an appropriate *a priori* model m_{apr} :

$$s_{\mathrm{MS}}(m) = \int_V \frac{(m - m_{\mathrm{apr}})^2}{(m - m_{\mathrm{apr}})^2 + e^2}\,\mathrm{d}v, \tag{11}$$

where e is the focusing parameter. It was shown by Portniaguine and Zhdanov (1999) that this functional minimizes the area of nonzero parameter distribution (minimizes the support of the inverse model), if e tends to zero: $e \to 0$. The focusing parameter characterizes the degree of sharpness of the boundary between the domains with the different slowness (Zhdanov 2002). If e is small ($e^2 \ll (m - m_{\mathrm{apr}})^2$), we generate an image with very sharp boundaries; otherwise an image may have a relatively smooth boundary. The principles of the optimal focusing parameter selection are formulated in Zhdanov and Tolstaya (2004).

4. Parametric functional minimization scheme

The solution of inverse problems is based on minimization of the parametric functional

$$P^{\alpha}(m) = (A(m) - d, A(m) - d)_D + \alpha s(m), \tag{12}$$

where $(\ldots,\ldots)_D$ denotes the inner product in the Hilbert space D of the data.

Zhdanov (2002, p 50) demonstrated that the stabilizing functionals we considered above can be written in the following way:

$$s(m) = (W_e(m - m_{\mathrm{apr}}), W_e(m - m_{\mathrm{apr}}))_M, \tag{13}$$

where $(\ldots,\ldots)_M$ denotes the inner product in the Hilbert space M of the model parameters, W_e is an operator of multiplication of the model parameters function $m(\mathbf{r})$ by the auxiliary function $w_e(\mathbf{r})$.

In the case of the minimum norm stabilizer, w_e is equal to 1. In the case of the minimum support stabilizer,

$$w_e(\mathbf{r}) = \frac{1}{[(m(\mathbf{r}) - m_{\mathrm{apr}}(\mathbf{r}))^2 + e^2]^{1/2}}. \tag{14}$$

For discrete model parameters, we can write, using the matrix notation,

$$s(m) = [\widehat{\mathbf{W}}_e(\mathbf{m} - \mathbf{m}_{\mathrm{apr}})]^T \widehat{\mathbf{W}}_e(\mathbf{m} - \mathbf{m}_{\mathrm{apr}}), \tag{15}$$

where the upper superscript 'T' denotes a transposed matrix, and $\widehat{\mathbf{W}}_e$ is a diagonal matrix defined, in the nontrivial case of the minimum support stabilizer, as

$$\widehat{\mathbf{W}}_e = \mathbf{diag}\left[\frac{1}{[(m - m_{\mathrm{apr}})^2 + e^2]^{1/2}}\right] = \mathbf{diag}[w_e]. \tag{16}$$

In the above formula, $\mathbf{diag}[w_e]$ is a diagonal matrix formed by the values of function w_e determined by the discrete values of the function $m(\mathbf{r})$ describing the model parameters. It is worth noting that, in this case, $\widehat{\mathbf{W}}_e$ depends on m!

According to the regularization theory, the goal is finding a quasi-solution of the inverse problem, m_{α}, such that

$$P^{\alpha}(m_{\alpha}, d) = \min. \tag{17}$$

Portniaguine and Zhdanov (1999) have developed a simplified approach to minimizing the parametric functional (17) with the minimum support stabilizer, using the so-called re-weighted regularized conjugate gradient (RRCG) method. In the framework of this approach, the variable weighting matrix $\mathbf{W}_e$ is precomputed on each iteration, $\mathbf{W}_e = \mathbf{W}_{en} = \mathbf{W}_e(\mathbf{m}_n)$, based on the values $\mathbf{m}_n$ obtained on the previous iteration. This linear transformation is updated after a fixed number of intermediate iterations, which is equivalent to the re-weighting of the model parameters. The advantage of this approach is in its simplicity. The disadvantage is due to re-weighting; the misfit and stabilizing functionals can change and even increase from iteration to iteration (Zhdanov 2002). In the present paper, we follow the approach developed by Ueda and Zhdanov (2003) and solve the same problem using the direct minimization of the Tikhonov parametric functional with the minimum support stabilizer.

In the general case, the solution of the minimization problem (17) can be obtained iteratively using a gradient-type method, which requires calculation of the gradient (or the first variation, δP^{α}) of the parametric functional on each iteration step. In a simple case of the minimum norm stabilizer, the corresponding equation for $\delta P^{\alpha}_{\mathrm{MN}}$ can be obtained by direct calculation:

$$\begin{aligned}\delta P^{\alpha}_{\mathrm{MN}} &= \delta[(Am - d, Am - d)_D + \alpha(m - m_{\mathrm{apr}}, m - m_{\mathrm{apr}})_M] \\ &= 2(\delta m, A^*(Am - d) + \alpha(m - m_{\mathrm{apr}}))_M,\end{aligned} \tag{18}$$

where δm is the perturbation of the model, and A^* is the adjoint operator determined by the formula

$$(Am, d)_D = (m, A^*d)_M.$$

In the case of the minimum support stabilizer, one can derive

$$\begin{aligned}\delta P^{\alpha}_{\mathrm{MS}} &= 2(\delta m, A^*(Am - d))_M \\ &\quad + 2\alpha(\delta(w_e(m - m_{\mathrm{apr}})), w_e(m - m_{\mathrm{apr}}))_M,\end{aligned} \tag{19}$$

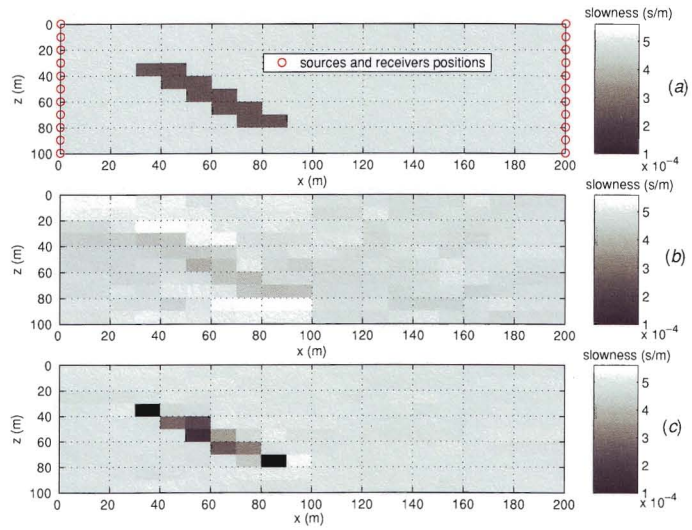

Figure 1. Model 1. A comparative study of the minimum norm inversion (*b*) and the minimum support inversion (*c*) for a crosswell tomography model 1 (panel (*a*) consisting of a dipping slab with 4 km s^{-1} seismic wave velocity embedded within a homogeneous background with 2 km s^{-1} velocity. The noise level is 1%. The parameters used for inversion are as follows. In the minimum norm inversion, $q = 0.85$, and α is modified every seven iterations. In the minimum support inversion, $e = 0.003$, $q = 0.99$, and α is modified every five iterations. Note that parameter q represents how much α changes from iteration to iteration according to equation (36).

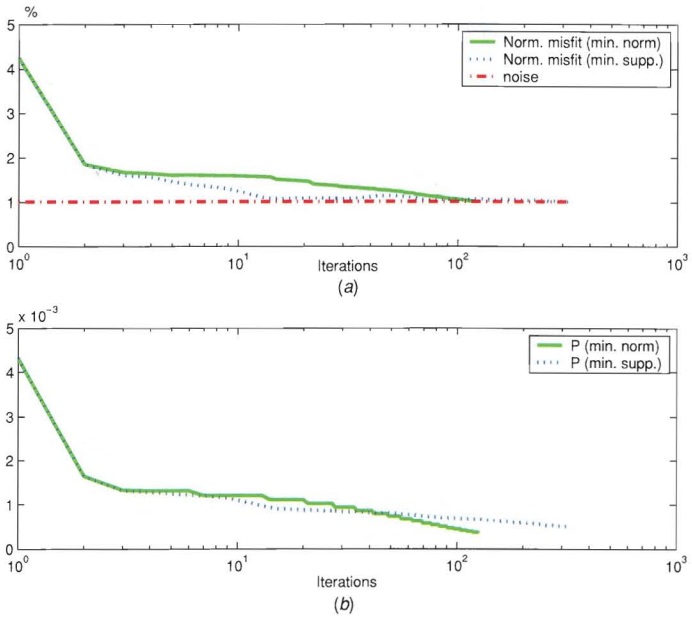

Figure 2. Panels (*a*) and (*b*) present the behaviour of the normalized misfits and parametric functionals versus iteration number during the inversion of the model shown in figure 1. The solid line describes the inversion process with the minimum norm stabilizer, while the dotted line describes the behaviour of the misfit and parametric functional for the minimum support minimization. The dash-dotted line in panel (*a*) shows the noise level.

where

$$\delta(w_e(m - m_{\text{apr}})) = w_e\delta m + w'_e(m - m_{\text{apr}})\delta m \qquad (20)$$

and

$$w'_e = -\frac{(m - m_{\text{apr}})}{((m - m_{\text{apr}})^2 + e^2)^{\frac{3}{2}}}. \qquad (21)$$

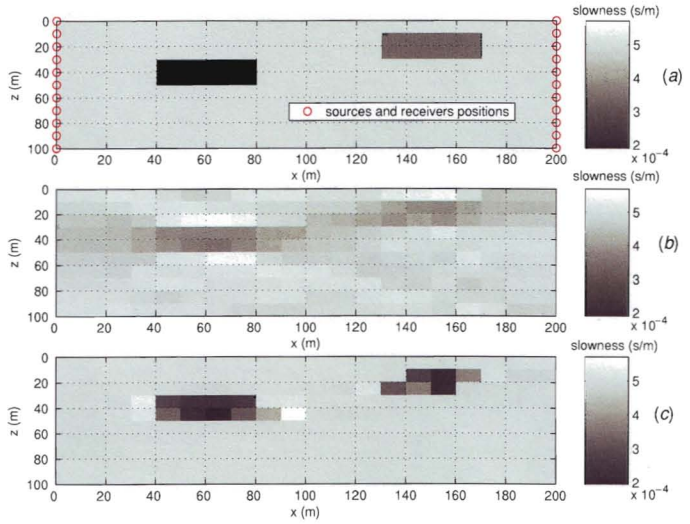

Figure 3. Model 2. A comparative study of the minimum norm inversion (*b*) and the minimum support inversion (*c*) for a crosswell tomography model (*a*) consisting of two bodies with 4 km s^{-1} and 3 km s^{-1} seismic wave velocity embedded within a homogeneous background with 2 km s^{-1} velocity. The noise level is 1%. The parameters used for inversion are as follows. In the minimum norm inversion, $q = 0.85$, and α is modified every seven iterations. In the minimum support inversion, $e = 0.003$, $q = 0.99$, and α is modified every five iterations.

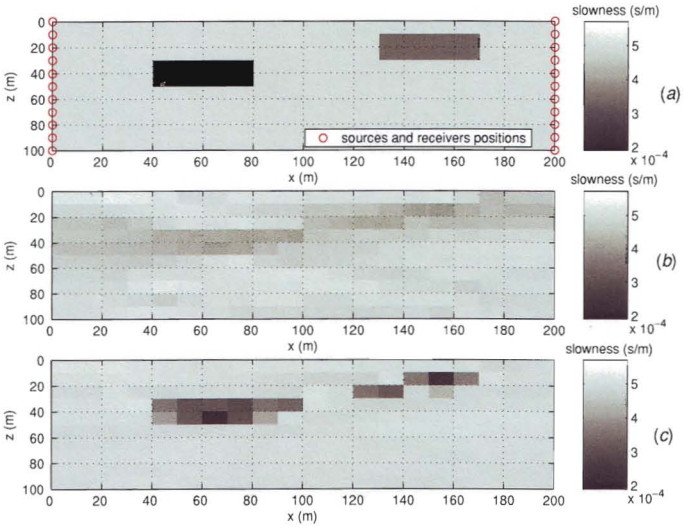

Figure 4. Model 2. A comparative study of the minimum norm inversion (*b*) and the minimum support inversion (*c*) for a crosswell tomography model (*a*) consisting of two bodies with 4 km s^{-1} and 3 km s^{-1} seismic wave velocity embedded within a homogeneous background with 2 km s^{-1} velocity. The noise level is 5%. The parameters used for inversion are as follows. In the minimum norm inversion, $q = 0.85$, and α is modified every seven iterations. In the minimum support inversion, $e = 0.003$, $q = 0.99$, and α is modified every five iterations.

Using the matrix notation, we write expressions (18) and (19) as

$$\delta P^{\alpha}_{\mathrm{MN}} = 2\delta\mathbf{m}^T[\widehat{\mathbf{A}}^T(\widehat{\mathbf{A}}\mathbf{m} - \mathbf{d}) + \alpha(\mathbf{m} - \mathbf{m}_{\mathrm{apr}})] \tag{22}$$

and

$$\delta P^{\alpha}_{\mathrm{MS}} = 2\delta\mathbf{m}^T[\widehat{\mathbf{A}}^T(\widehat{\mathbf{A}}\mathbf{m} - \mathbf{d}) + \alpha(\widehat{\mathbf{W}}_e + \widehat{\mathbf{W}}'_e\,\mathbf{diag}(m - m_{\mathrm{apr}}))\widehat{\mathbf{W}}_e(\mathbf{m} - \mathbf{m}_{\mathrm{apr}})], \tag{23}$$

with $\widehat{\mathbf{W}}_e = \mathbf{diag}(w_e)$ and $\widehat{\mathbf{W}}'_e = \mathbf{diag}(w'_e)$.

Following the general scheme of the gradient-type methods (Zhdanov 2002), in order to obtain $\delta P^{\alpha} \leqslant 0$, we select

$$\delta\mathbf{m} = -k^{\alpha}\mathbf{l}^{\alpha}(\mathbf{m}), \tag{24}$$

where k^{α} is a positive real number, and $\mathbf{l}^{\alpha}$ is the column vector defining the direction of the steepest ascent of the parametric functional.

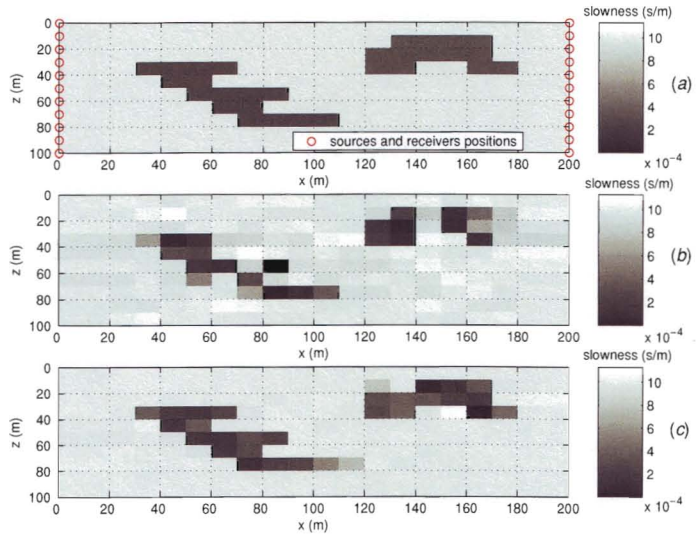

Figure 5. Model 3. A comparative study using the minimum support inversion of the crosswell seismic tomographic data simulated for the complex model presented in panel (*a*). Panel (*b*) presents the inversion result without the model parameter weights, and panel (*c*) shows the same result with the model parameter weights. The parameters used for inversion are as follows. In inversion without W_m, $e = 0.003$, $q = 0.99$, and α is modified every iteration. In inversion with W_m, $e = 0.003$, $q = 0.99$, and α is modified every five iterations.

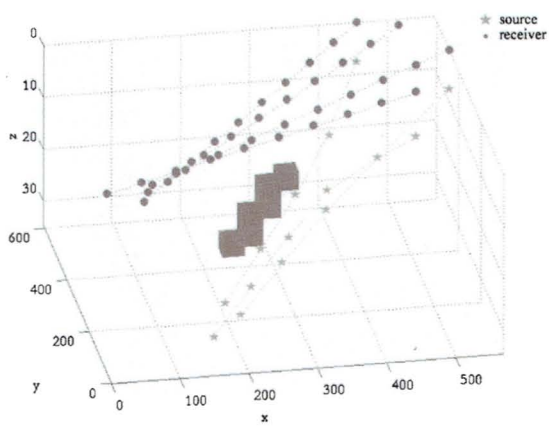

Figure 6. Model 4 consists of a dipping slab with 4 km s^{-1} seismic wave velocity embedded within a homogeneous background (2 km s^{-1}).

In the case of the minimum norm stabilizer,

$$\mathbf{l}^{\alpha} = \widehat{\mathbf{A}}^T(\widehat{\mathbf{A}}\mathbf{m} - \mathbf{d}) + \alpha(\mathbf{m} - \mathbf{m}_{\text{apr}}). \tag{25}$$

The direction of the steepest ascent for the parametric functional with the minimum support stabilizer is

$$\mathbf{l}^{\alpha} = \widehat{\mathbf{A}}^T(\widehat{\mathbf{A}}\mathbf{m} - \mathbf{d}) + \alpha(\widehat{\mathbf{W}}_e + \widehat{\mathbf{W}'}_e\,\mathbf{diag}(m - m_{\text{apr}}))\widehat{\mathbf{W}}_e(\mathbf{m} - \mathbf{m}_{\text{apr}}). \tag{26}$$

Using the appropriate expression amongst (25) and (26) in the formulae for the conjugate gradient method, we have the following algorithm (Zhdanov 2002) of the regularized conjugate gradient inversion (RCG):

$$\mathbf{r}_n = \widehat{\mathbf{A}}\mathbf{m}_n - \mathbf{d}, \tag{27}$$

$$\mathbf{l}_n^{\alpha_n} = \mathbf{l}_{\text{MN}}^{\alpha_n}(\mathbf{m}_n) = \widehat{\mathbf{A}}^T\mathbf{r}_n + \alpha(\mathbf{m}_n - \mathbf{m}_{\text{apr}}) \quad \text{(minimum norm)} \tag{28}$$

or

$$\mathbf{l}_n^{\alpha_n} = \mathbf{l}_{\text{MS}}^{\alpha_n}(\mathbf{m}_n) = \tag{29}$$

$$\widehat{\mathbf{A}}^T\mathbf{r}_n + \alpha(\widehat{\mathbf{W}}_e + \widehat{\mathbf{W}'}_e\,\mathbf{diag}(m - m_{\text{apr}}))\widehat{\mathbf{W}}_e(\mathbf{m} - \mathbf{m}_{\text{apr}}), \tag{30}$$

(minimum support) (31)

$$\beta_n^{\alpha_n} = \frac{\|\mathbf{l}_n^{\alpha_n}\|^2}{\|\mathbf{l}_{n-1}^{\alpha_n}\|^2}, \tag{32}$$

$$\widetilde{\mathbf{l}}_n^{\alpha_n} = \mathbf{l}_n^{\alpha_n} + \beta_n^{\alpha_n}\widetilde{\mathbf{l}}_{n-1}^{\alpha_n}, \qquad \widetilde{\mathbf{l}}_0^{\alpha_n} = \mathbf{l}_0^{\alpha_n}, \tag{33}$$

$$\widetilde{\mathbf{k}}_n^{\alpha_n} = \frac{\widetilde{\mathbf{l}}_n^{\alpha T}\mathbf{l}_n^{\alpha_n}}{\|\widehat{\mathbf{A}}\widetilde{\mathbf{l}}_n^{\alpha_n}\|^2 + \alpha_n\|\widetilde{\mathbf{l}}_n^{\alpha_n}\|^2}, \tag{34}$$

$$\mathbf{m}_{n+1} = \mathbf{m}_n - \widetilde{k}_n^{\alpha}\widetilde{\mathbf{l}}_n^{\alpha_n}. \tag{35}$$

In the last formulae vectors $\mathbf{l}_n^{\alpha_n}$ are the gradient directions, while vectors $\widetilde{\mathbf{l}}_n^{\alpha_n}$ are the conjugate directions. The length of a step $k_n^{\alpha_n}$ is determined using a linear line search on every iteration.

The regularization parameter α describes a trade-off between the best fitting and the most reasonable stabilization. If α is selected too small, the minimization of $P^{\alpha}(\mathbf{m})$ is equivalent to the minimization of the misfit functional $\phi(\mathbf{m})$, thus we do not have regularization. When α is too big, minimization of $P^{\alpha}(\mathbf{m})$ is equivalent to the minimization of the stabilizer functional $s(\mathbf{m})$, which will force the solution to be closer to the *a priori* model.

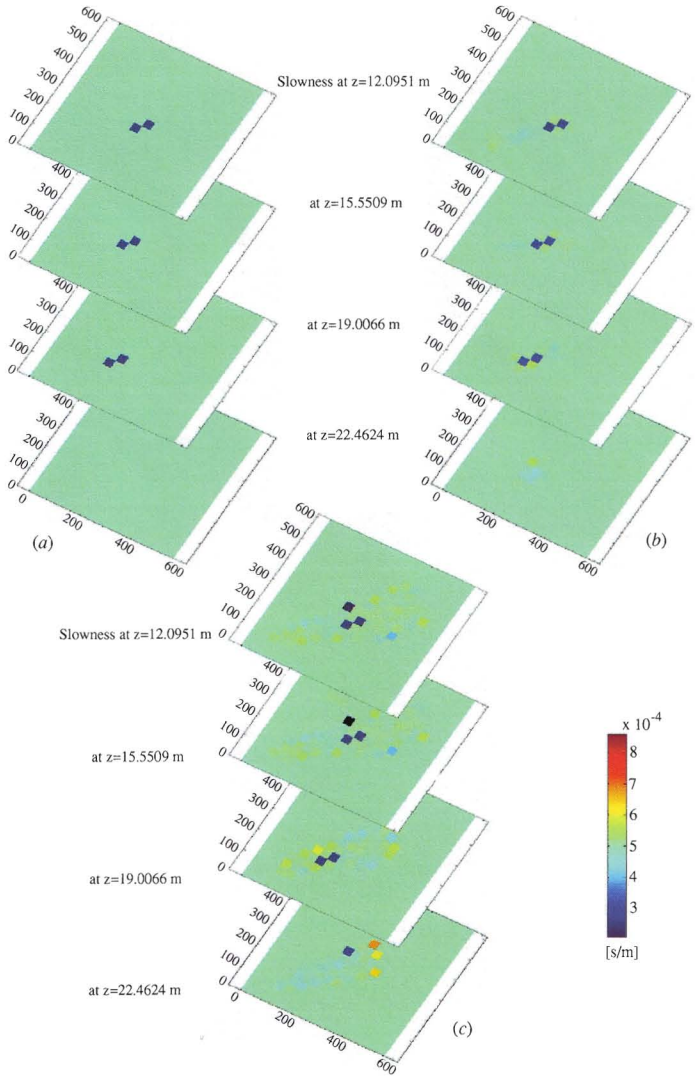

Figure 7. A comparative study of minimum support (*b*) and minimum norm (*c*) inversion of travel times from model 4 (figure 1). Panel (*a*) shows the same plots for the true model.

In our algorithm, the regularization parameter α is selected using the adaptive regularization (Zhdanov 2002, p 154). This means that α is updated during the process of iterative inversion in the following manner. The initial iteration is run with $\alpha_0 = 0$. In the following iterations

$$\alpha_n = \alpha_1 q^{n-1}, \qquad n = 1, 2, \ldots, \qquad 0 < q < 1, \quad (36)$$

where α_n are the subsequent values of the regularization parameter, and α_1 is determined, after the first iteration, as the ratio

$$\alpha_1 = \frac{\|A(\mathbf{m}_1) - d\|^2}{s(\mathbf{m}_1)}, \quad (37)$$

and m_1 is the model obtained after the first iteration.

Note that the regularization parameter α can be modified not on every iteration, but after every Nth iteration, where N is usually selected from 1 to 10. The minimization process is terminated when the misfit condition is reached:

$$\|\widehat{\mathbf{A}}\mathbf{m}_n - \mathbf{d}\| = \delta, \quad (38)$$

where δ is the noise level in the observed data.

5. Model parameter weights

It was demonstrated in the monograph by Zhdanov (2002) that it is important to use the appropriate weights for the model parameters in order to have an efficient inversion algorithm. The model weighting matrix $\widehat{\mathbf{W}}_m$ is usually selected based

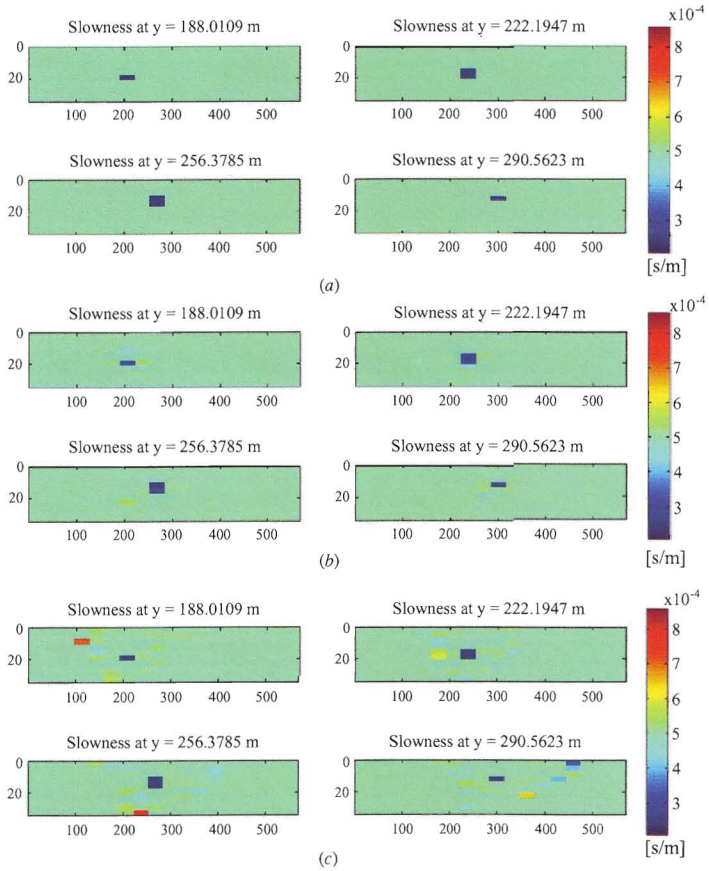

Figure 8. A comparative study of minimum support (*b*) and minimum norm (*c*) inversion of travel times from *model 1* (figure 1). Panel (*a*) shows the same plots for the true model.

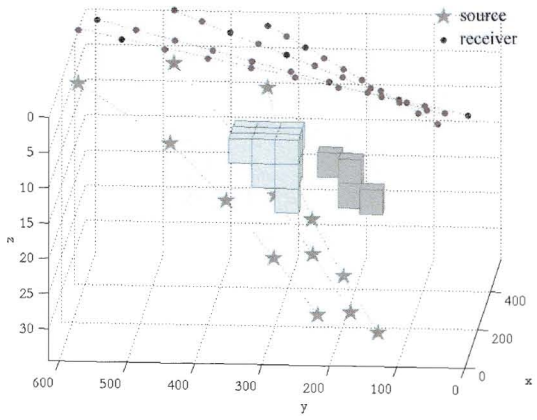

Figure 9. Model 5 consists of two anomalies with, respectively, 6 km s^{-1} and 5 km s^{-1} seismic wave velocity embedded within a homogeneous background (5.5 km s^{-1}). Transmitter–receiver configuration is the same as in model 4 (figure 9) (6).

on the sensitivity analysis of the geophysical method. In particular, the weighting matrix $\widehat{\mathbf{W}}_m$ selected as the square root of the sensitivity matrix provides the uniform sensitivity of the data to the different model parameters (Zhdanov 2002):

$$\widehat{\mathbf{W}}_m = \mathbf{diag}(\widehat{\mathbf{A}}^T\widehat{\mathbf{A}})^{\frac{1}{2}} = \mathbf{diag}\left(\sqrt{\sum_i (A_{ij})^2}\right). \tag{39}$$

The physical meaning of this choice is evident if we take into account that $\sum_i A_{ij}$ is the sum of the distances that every ray travels in the pixel jth. These weights really make the sensitivity of the travel time uniform to the effect of every cell of the grid.

In order to include the model parameter weights in the RCG algorithm described above, we introduce the weighted model parameters $\mathbf{m}^w$ according to the formula

$$\mathbf{m}^w = \widehat{\mathbf{W}}_m \mathbf{m}. \tag{40}$$

Now we solve the problem of the parametric functional minimization in the space of the weighted parameters $\mathbf{m}^w$. In this situation, the forward operator is modified as

$$\widehat{\mathbf{A}}_w \mathbf{m}^w = \widehat{\mathbf{A}}\widehat{\mathbf{W}}_m^{-1}\mathbf{m}^w. \tag{41}$$

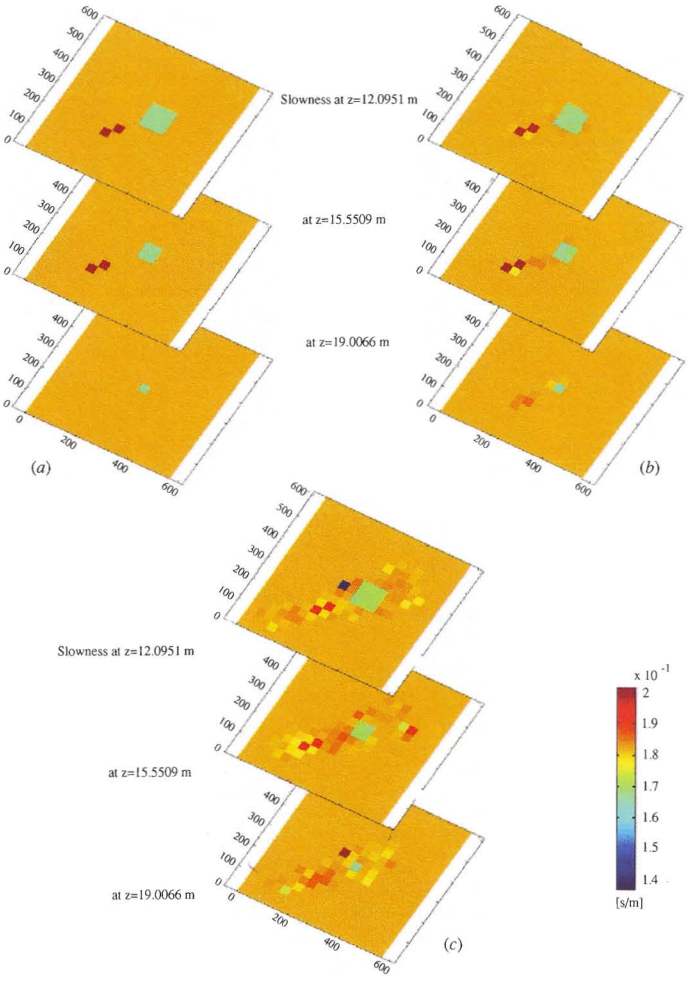

Figure 10. A comparative study of minimum support (*b*) and minimum norm (*c*) inversion of travel times from model 5 (figure 9). Panel (*a*) shows the same plots for the true model.

To obtain the original model parameters, we have to apply inverse weighting to the result of the parametric functional minimization in the space of the weighted parameters:

$$\mathbf{m} = \widehat{\mathbf{W}}_m^{-1}\mathbf{m}^w. \tag{42}$$

6. 2D crosswell seismic tomography problems

Let us consider synthetic model 1 of the crosswell travel-time tomography, shown in figure 1. The sources and the receivers are equally spaced and placed in two wells at the left and right boundaries of the model (11 sources and 11 receivers in every well). Synthetic 'observed' data for this model were computed using the Fermat principle discussed above (equations (4) and (7)). In order to simulate a practical situation with the noisy observed data, the synthetic data were contaminated by normally distributed random noise, $\delta\mathbf{d}$, according to the formulae

$$\mathbf{d} = \widehat{\mathbf{A}}\mathbf{m}^{\text{true}} + \delta\mathbf{d}, \tag{43}$$

and

$$\delta\mathbf{d} = p\langle\widehat{\mathbf{A}}\mathbf{m}^{\text{true}}\rangle\widehat{\mathbf{n}}, \tag{44}$$

where $\mathbf{m}^{\text{true}}$ is the true model, $\langle\widehat{\mathbf{A}}\mathbf{m}^{\text{true}}\rangle$ is the mean value of $\widehat{\mathbf{A}}\mathbf{m}^{\text{true}}$, p is the percentage of noise, and $\widehat{\mathbf{n}}$ is a diagonal matrix of normally distributed random numbers with the mean value equal to zero and standard deviation equal to one. This choice for noise distribution makes the 'observed' synthetic data more realistic and harder to invert than in the case of uniformly distributed noise.

Panel (*a*) in figure 1 shows the true model of the slowness distribution. Panel (*b*) presents the inversion result obtained with the minimum norm stabilizer. The grid spacing used for inversion is 10 m × 10 m. The image is unfocused and diffused because the minimum norm solution is characterized

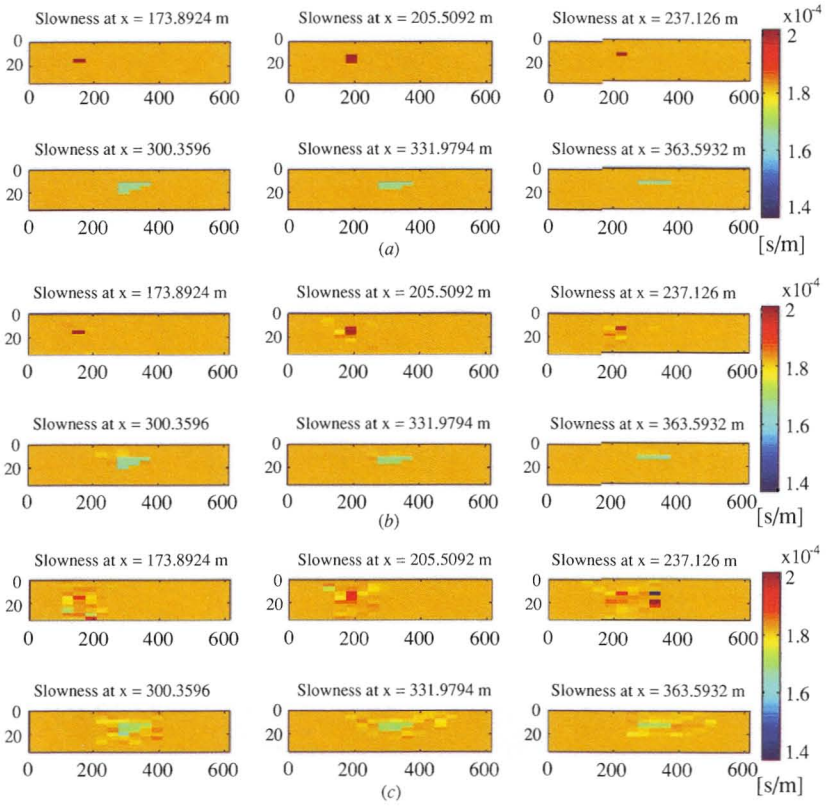

Figure 11. A comparative study of minimum support (*b*) and minimum norm (*c*) inversion of travel times from model 5 (figure 9). Panel (*a*) shows the same plots for the true model.

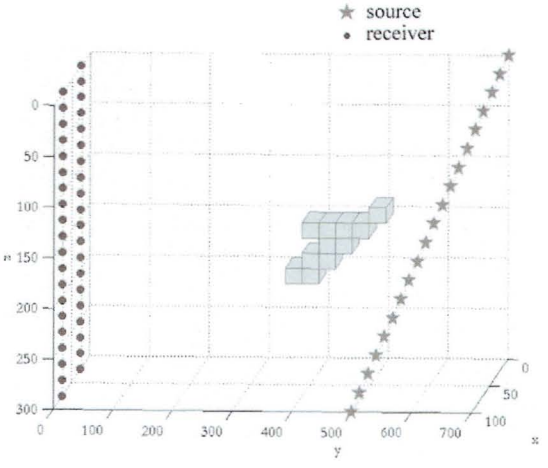

Figure 12. Model 6 consists of a quite complex target with 6 km s^{-1} seismic velocity embedded within a homogeneous background (5 km s^{-1}).

by relatively smooth distribution of the model parameters. Panel (*c*) shows the inversion result obtained with the minimum support stabilizer. In figure 2, panels (*a*) and (*b*) present the behaviour of the normalized misfits and parametric functionals versus iteration number for model shown in figure 1. The solid lines describe the inversion process with the minimum norm stabilizer, while the dotted lines describe the behaviour of the misfit and parametric functional for the minimum support minimization. Both iteration processes are terminated when the misfit reaches the level of noise, p, which is 1% for this numerical example. It is clear that using a minimum support stabilizer improves the image resolution dramatically (figure 1(*c*)). Note that the synthetic noise that we used in this and other experiments was not white random noise, but normally distributed random noise.

Figures 3 and 4 show the inversion results for the same model 2 consisting of two blocks with different seismic wave slowness, but for data contaminated by different noise levels, 1% and 5%, respectively. What is interesting is that the minimum support inversion applied to data with 5% noise (figure 4(*c*)) still provides a better result than the minimum norm inversion of data with 1% noise (figure 3(*b*)). The last numerical test illustrates the importance of the model parameter weights. Figure 5 presents the seismic tomography results obtained for model 3 with a quite complicated shape and slowness distribution. We apply the minimum support

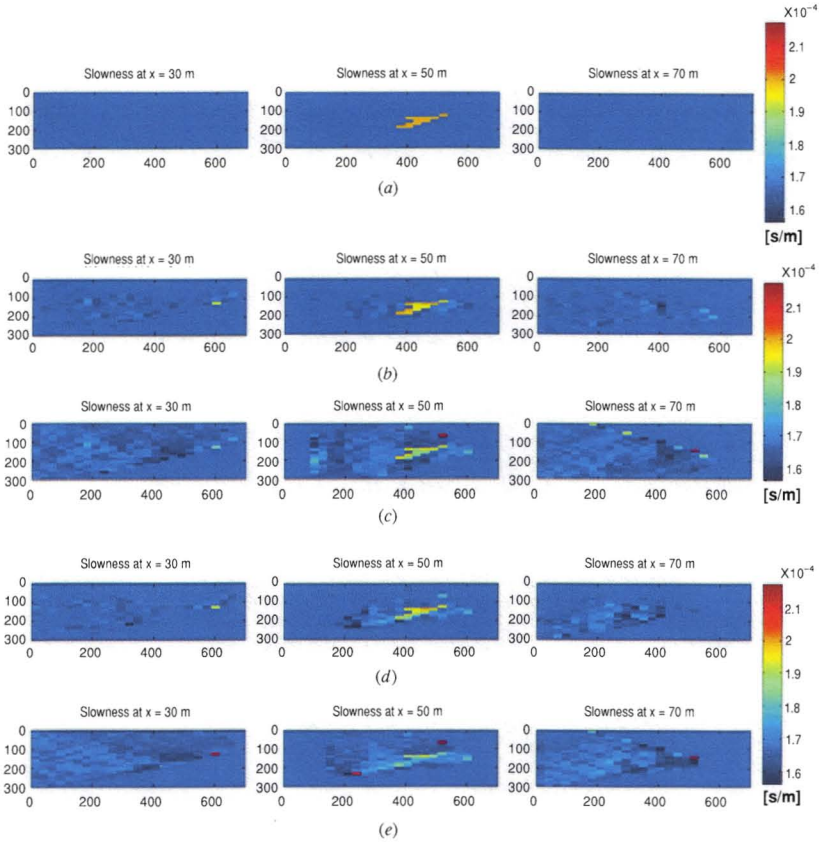

Figure 13. A comparative study of minimum support and minimum norm inversion of data from model 6 (figure 12). Panel (*a*) shows the true model; in panels (*b*), (*d*), it is possible to see minimum support results obtained using, respectively, 20 and only 12 transmitters; panels (*c*), (*e*) show minimum norm results obtained from the same two data sets (20 and 12 transmitters).

inversion without the model parameter weights (figure 5(*b*)) and with the model parameter weights (figure 5(*c*)). This test shows that model parameter weights based on the sensitivities provide a better resolution of the bodies. Note that the grid spacing used for inversion for models 2 and 3 is the same: 10 m × 10 m.

7. 3D crosswell seismic tomography problems

In this section, we use the same algorithm as above, but apply it to 3D data. We compare the results of regularized inversion performed with the two stabilizing functionals introduced above: the minimum norm, s_{MN}, and the minimum support, s_{MS}, stabilizers. Let us consider a synthetic 3D model 4 of the travel-time tomography, shown in figure 6. Fifteen sources are located in three boreholes that are not vertical and not straight while forty receivers are at the ground level; this model consists of a dipping slab with 4 km s^{-1} seismic wave velocity embedded within a background with 2 km s^{-1} velocity. Figures 7(*b*) and (*c*) show the inversion results along the z constant planes obtained using, respectively, s_{MS} and s_{MN}, while panel (*a*) in this figure presents the horizontal sections of a true model. The grid spacing used for inversion is 31.6 m × 34.2 m × 3.4 m in the x, y, and z directions, respectively.

If we compare these images with the true model (figure 7(*a*)), we can see that the minimum norm result is unfocused and diffused because this stabilizer generates a solution characterized by relatively smooth distribution of the model parameters. Figure 8 shows the slices of the same results along y constant planes.

Let us analyse the inversion results for model 5 (figures 9–11). It is a quite complicated model: the source–receiver configuration is the same as in the former example; there are two anomalies with different velocities (5 km s^{-1} and 6 km s^{-1}) enclosed in a background with 5.5 km s^{-1}. The grid spacing used for this model is the same as for model 4.

Detecting the small low-velocity anomaly is particularly difficult; in fact, it is shielded by the bigger high-velocity anomaly. We would like to point out that s_{MS} can reconstruct

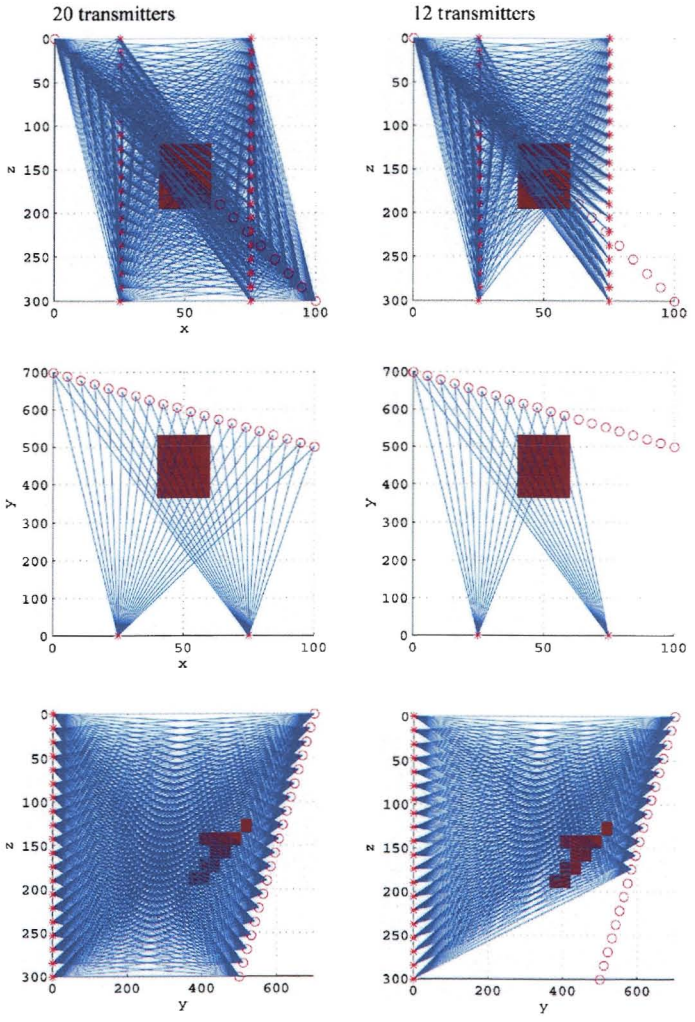

Figure 14. Ray distributions for model 6. Left panels show the vertical and horizontal projections of the rays for the case with 20 sources, while the right panels present the same pictures for the case with only 12 sources.

properly not only the shape but also the velocity value of both of the bodies (figures 10(*b*) and 11(*b*)). This would be even clearer if we analyse the two inversion results using two different colour scales that fit better the two sets of model parameter values. In fact, in order to plot all figures with the same colour scale, we use the colour range of the minimum norm case because it is the widest.

In model 6 (figures 12 and 13), the parameter value range for the minimum norm is much wider but, in these figures, we plot the data using a colour scale that goes from 1.562×10^{-4} s m^{-1} (6.4 km s^{-1}) to 2.173×10^{-4} s m^{-1} (4.6 km s^{-1}) and we clamp the values outside this interval to the two limit colours. The goal of this last example is to illustrate that s_{MS} can help to reconstruct targets properly even in those situations where ray coverage is far from optimal. The grid spacing used for inversion for model 6 is 20 m $\times$ 28 m $\times$ 15 m in the x, y, and z directions, respectively. In figures 13(*b*) and (*c*), we can see the results of minimum support and minimum norm inversion if we use data from all 20 transmitters; in this case, even s_{MN} provides a good result. If we use a transmitter borehole that is not so deep (thus we use only the first 12 sources) we can see (figure 13(*d*) that s_{MS} still provides good resolution of the body while this is not true for s_{MN} inversion (figure 13(*e*)). The ray distributions for model 6 are displayed in figure 14. Left panels show the vertical and horizontal projections of the rays for the case with 20 sources, while the right panels present the same pictures for the case with only 12 sources. One can see that we have poorer ray coverage for the model with 12 sources in comparison with the model where we have 20 sources. Thus, we can conclude that

the method works well even under the condition of relatively poor ray coverage.

8. Conclusions

In this paper, we have developed a new tomographic method based on application of a minimum support (MS) stabilizer to the crosswell travel-time inverse problem. We have investigated different methods of regularized inversion in interpretation of travel-time tomography data. The results of this work demonstrate that minimum support inversion improves resolution of the tomographic imaging and provides a clear and focused image of targets with sharp boundaries between areas with different seismic wave velocities.

It is also shown that this kind of inversion is quite robust to noise. It allows us to recover an accurate image even in the presence of a relatively high level of noise in the data. We also show the importance of using the appropriate model parameter weights in order to obtain a good image of anomalous structure.

Finally, this work demonstrates that the new tomographic inversion with the MS stabilizer provides good results even with a poor ray coverage, when the traditional methods with the maximum smoothness stabilizing functional fails. In practice, this result means that with the new inversion method one can use a transmitter borehole that is not as deep as is required by conventional travel-time tomography.

Acknowledgments

The authors acknowledge the support of the University of Utah Consortium for Electromagnetic Modeling and Inversion (CEMI), which includes Baker Atlas Logging Services, BGP China National Petroleum Corporation, BHP Billiton World Exploration Inc, EMGS, ENI SpA, ExxonMobil Upstream Research Company, INCO Exploration, Newmont, Norsk Hydro, Rio Tinto-Kennecott, Petrobras, Schlumberger Oilfield Services, Shell International Exploration and Production Inc, Statoil, Sumitomo Metal Mining Co, and Zonge Engineering and Research Organization. One of the authors (GV) wishes to express gratitude to the Dipartimento di Scienze della Terra, Università di Ferrara and to the Istituto Nazionale di Oceanografia e di Geofisica Sperimentale (OGS). GV is also very grateful to Alessandro Drago.

References

Geman D and Reynolds G 1992 *IEEE Trans. Pattern Anal. Mach. Intell.* **4** 367–83
Geman D and Yang C 1995 *IEEE Transactions on Image Processing* pp 932–46
Hyndman D W and Harris J M 1996 *Geophysics* **61** 1728–37
Lee D S, Stevenson V M, Johnston P F and Mullen C E 1995 *Geophysics* **60** 660–6
Lobel P, Blanc-Feraud L, Pichot C and Barlaud M 1997 *Inverse Problems* **3** 403–10
Portniaguine O and Zhdanov M S 1999 *Geophysics* **64** 874–87
Pratt R G, McGaughey W J and Chapman C H 1993 *Geophysics* **58** 1748–63
Rechtien R D, Greenfield R J and Ballard R F 1995 *Geophysics* **60** 76–86
Tikhonov A N and Arsenin V Y 1977 *Solution of Ill-Posed Problems* (Palm Beach, FL: Winston)
Ueda T and Zhdanov M S 2003 *Proc. Ann. Mtg Consortium for Electromagnetic Modeling and Inversion* pp 19–39
Vogel C R 1997 Nonsmooth regularization *Inverse Problems in Geophysical Applications* ed H W Engl, A K Louis and W Rundell (Philadelphia: SIAM) pp 1–11
Williams M C, Leighton V L, Vassiliou A A, Tan H, Nemeth T, Dale V and Howlett D L 1997 *The Leading Edge* **16** 285–91
Wong J 2000 *Geophysics* **65** 1900–7
Wright J, Harrell H C, Wong J, Nelson J S and Gibbs D 1988 *58th Ann. Int. Mtg Soc. Expl. Geophys.* Expanded Abstracts pp 370–3
Yamamoto T, Nye T and Kuru M 1994 *Geophysics* **59** 1530–41
Zhdanov M S 2002 *Geophysical Inverse Problems and Regularization Theory* (Amsterdam: Elsevier)
Zhdanov M S and Tolstaya E 2004 *Inverse Problems* **20** 937–52